Chapter 2

Current Source Density Analysis of Ongoing Neural Activity: Theory and Application

Yonghong Chen, Mukesh Dhamala, Anil Bollimunta, Charles E. Schroeder, and Mingzhou Ding

Abstract

Current source density (CSD) is the second spatial derivative of the local field potential (LFP). CSD analysis has been used extensively to localize the pattern of transmembrane current flow in neuronal ensembles. For brain responses to repeated external stimulation, the LFP data are epoched and averaged across an ensemble of trials, from which the CSD profile is then derived. For spontaneous brain activity, however, the lack of an external triggering event makes ensemble average difficult, hampering the investigation of such important cognitive functions as anticipatory attention and working memory. In this chapter, we describe a new method called phase realigned averaging technique (PRAT), which can overcome this difficulty and achieve CSD profiles on a frequency-by-frequency basis. The method is first validated on simulation examples and then applied to LFP recordings from a monkey performing an intermodal selective attention task.

Key words: Local field potential, Current source density analysis, Alpha oscillations, Cortical column

1. Introduction

Local field potentials (LFPs) are an important index of brain activity. Generated by electrical currents flowing across cell membranes, LFPs, together with population spikes, provide complementary measures of ensemble neural dynamics at both the input and the output level. Typically, LFPs are measured against a distant reference and are thus vulnerable to volume-conducted far-field effects. The second spatial derivative of LFPs, called the current source density (CSD), eliminates this problem and has the ability of more precisely localizing transmembrane currents than LFPs. To date, CSD analysis has been mainly applied to stimulus-evoked neural

Robert P. Vertes and Robert W. Stackman Jr. (eds.), *Electrophysiological Recording Techniques*, Neuromethods, vol. 54,
DOI 10.1007/978-1-60327-202-5_2,

responses. Following repeated experiments, LFP data are epoched and averaged across an ensemble of trials, triggered on some external event such as stimulus onset. The CSD profile is then computed on the averaged LFPs. This approach, widely practiced, has yielded valuable insights into the neuronal mechanisms behind sensory as well as higher order cognitive processes (1–4).

Neurons in the brain are spontaneously active even in the absence of sensory stimulation. This ongoing neural activity, rich in oscillatory content, provides a window into such important brain functions as anticipation, working memory, and top-down deployment of attention (5, 6). To date, characterization of ongoing brain activity has mainly relied on time series techniques. How to extend CSD analysis to ongoing neural activity remains a challenge. The lack of an external trigger makes ensemble averaging difficult to achieve. Meanwhile, single-trial CSDs are too noisy to be a reliable indicator of meaningful neural events. In this chapter, we seek to develop a novel method called the phase realigned averaging technique (PRAT) to overcome this problem. The method is formulated in the spectral domain and can reveal CSD profiles in depth recordings on a frequency-by-frequency basis. Simulated examples are used to demonstrate its effectiveness. It is then applied to laminar LFPs sampled with a multi-contact electrode placed in the inferotemporal cortex of a macaque monkey performing an intermodal selective attention task.

2. Theoretical Background

CSD analysis was first introduced in 1950s (7, 8). Subsequent publications elucidated its theoretical basis and range of applicability (1, 3, 4, 9). A standard CSD analysis has several simplifying assumptions: ohmic conductive medium, constant extracellular conductivity, homogeneous in-plane neuronal activity, and equidistant laminar electrode contacts (1). As a result of the continuity condition in current flow, the CSD $I(x,y,z)$ in a small volume element is defined as the divergence of current flow density $\mathbf{J}$ from the surface of that element. Under the assumption of a purely ohmic conductive medium, it can be related to the negative of the Laplacian of the field potential $\Phi(x,y,z)$ (1, 3):

$$I = -\nabla(\sigma \nabla \Phi), \tag{1}$$

where σ is the conductivity tensor, positive I represents an outgoing current (source), and negative I an incoming current (sink). This relationship also incorporates quasi-static approximations in the Maxwell's equations (1, 10). Since σ is symmetric, it can be made diagonal through a linear transformation (9). If we further

assume that (1) the dendrites are elongated along the *z*-direction, (2) σ is homogeneous, and (3) the dominant current flows are along the elongated structures only, (2.1) reduces to:

$$I = -\sigma_z \partial^2 \Phi / \partial z^2, \tag{2}$$

where the *z*-direction is perpendicular to the cortical surface and $\sigma_z = \sigma$ is a constant.

Experimentally, the spatiotemporal LFPs denoted by $\psi(z, t)$ are generally recorded using a linear array electrode with multiple equally spaced recording contacts sampling activity from all six layers of the cortex. The second spatial derivative in (2.2) can be estimated by the following three-point finite-difference approximation:

$$\frac{\partial^2 \psi(z,t)}{\partial z^2} \approx \frac{\psi(z+h,t) - 2\psi(z,t) + \psi(z-h,t)}{h^2} \tag{3}$$

where h is the inter-electrode spacing. The CSD profiles are obtained by the negative of this derivative at the N–2 electrode contact positions. Here N is the number of electrode contacts, which are also referred to as channels in this chapter. The profiles at the first and the last electrode contact position can be estimated by extrapolating potential fields, but are usually left undefined.

3. Phase Realigned Averaging Technique

Physiological data are noisy. Single-trial CSD profiles are generally not very informative in identifying the precise patterns of transmembrane current flow. The signal-to-noise ratio can be improved by averaging over an ensemble of trials. For ongoing brain activity, this averaging procedure is not readily implementable because of the absence of an external trigger (e.g. stimulus onset) for trial alignment. Here we propose a method in the frequency domain to overcome this problem. Consider a LFP dataset recorded with a multicontact linear electrode. Let $\psi_m(z, t)$ be the data from the m-th trial, where the variable z denotes the electrode contact, t the time, and $m = 1, 2, 3, \ldots, M$ with M being the total number of trials. According to Fourier's theorem, $\psi_m(z, t)$ can be written as the linear superposition of sinusoids of different frequencies. The phase information at frequency f is obtained by fitting $x(t) = a_1 \sin(2\pi ft) + a_2 \cos(2\pi ft)$ to $\psi_m(z, t)$. After extracting the parameters a_1 and a_2, the phase (θ_m) for the m-th trial at frequency f is given by $\tan^{-1}(a_1 / a_2)$. Designating certain value of the phase as the trigger, all trials can be realigned according to this trigger. Averaging the realigned trials leads to the averaged LFP for this electrode contact. This is the essence of the method.

To realign the data from the whole electrode array, apply the following algorithm:

1. Choose a reference electrode contact or channel and estimate the phase at frequency f for all M trials. The reference channel is usually the channel with maximum signal power at f.
2. Shift each trial m by its delay $\theta_m/2\pi f$ for the data in all the channels. The relation among the data from different channels is preserved.
3. Repeat step 2 for all trials.
4. Average over the realigned trials to obtain $<\psi(z,t^*)>$:

$$<\psi(z,t^*)> = \frac{1}{M}\sum_{m=1}^{M}\psi_m(z,t-\theta_m/2\pi f), \tag{4}$$

   where t^* is the adjusted time as the shifting operation disrupts the original physiological time.
5. Compute CSD profiles at frequency f as the negative of the second spatial derivative of $<\psi>$:

$$I \propto -<\psi>'' = -\frac{\partial^2 <\psi>}{\partial z^2}. \tag{5}$$

   The second derivative can be approximated by the finite difference formula in (3).

This method will be henceforth referred to as the PRAT. The resulting LFP and CSD profile will be referred to PRAT-LFP and PRAT-CSD, respectively. By scanning across the frequency spectrum of interest, one can analyze the current sources at different frequencies. See Csicsvari et al. (11) for a similar method based on band-pass filtering.

4. Simulations

Mathematical models are used to generate spontaneous spatiotemporal signals similar to that recorded in physiological experiments. The PRAT algorithm is then used to perform CSD analysis. By comparing the PRAT-CSD pattern with the corresponding mathematical functions, we are able to assess the validity of our method. Obviously, such a direct cross-validation is not possible in the analysis of real physiological data where the answer is not known a priori.

4.1. The Model

Experimentally, the data to be analyzed come from a cortical column. Here a cortical column is represented by the unit interval.

The transmembrane current is assumed to have a sinusoidal profile containing a source and a sink: $a_z \cos(2\pi f_z z + \theta_z)$, where a_z, f_z, θ_z (=$-\pi/2$) are amplitude, frequency, and phase. This term is referred to as the spatial dynamics term. Solving the differential equation

$$\frac{\partial^2 \varphi}{\partial z^2} = a_z \cos(2\pi f_z z + \theta_z),$$

we obtain

$$\phi(z) = C_1 z + C_2 - a_z \cos(2\pi f_z z + \theta_z) / (2\pi f_z)^2,$$

where C_1 and C_2 are constants. The temporal dynamics $\Psi(t)$ is modeled in two different ways: (1) a 10 Hz sinusoidal function $a_t \sin(2\pi f_t t + \theta_t)$ and (2) a second-order autoregressive process [AR(2)]: $\Psi(t) = \alpha\Psi(t-1) + \beta\Psi(t-2) + \xi(t)$, with α = 0.6, β = –0.9, and $\xi(t)$ being a white Gaussian noise. Like the 10-Hz sinusoid, the AR(2) process chosen this way also has a spectral peak at 10 Hz. Multiplying the space- and time-dependent functions and adding noise, we generate spatiotemporal LFP signals $\psi(z, t)$:

$$\psi(z,t) = \varphi(z)\psi(t) + \eta(z,t), \quad (6)$$

where $\eta(z, t)$ is a stochastic process with long-range power law (power α 1/frequency) correlation in all channels as well as random amplitude Gaussian noise in different channels (12). This choice is motivated by the observation that $1/f$ spectra are commonly observed in EEG and LFP recordings from the mammalian cortex (13–15).

4.2. CSD Analyses with PRAT

The above models were simulated and these data were assumed to be acquired by a multi-electrode with 14 equally spaced contacts. Figures 1 and 2 show the results for the two different temporal functions, 10-Hz sinusoid and AR(2), respectively. In both figures, panel (a) gives the color-coded power spectra at different contacts or channels (vertical axis) where oscillation at 10 Hz is clearly seen; panel (b) displays the superposition of 500 trials with random initial phases at the reference contact denoted by z_k; panel (c) shows the same 500 trials after phase realignment; panel (d) is the PRAT-LFP. The time label is from –100 to 0 ms. This label is motivated by the fact that, in the next section, experimental data from the prestimulus time period will be considered where the stimulus onset is defined as 0 ms. It is evident that the PRAT-LFPs in Figs. 1d and 2d are not able to reveal the underlying current/source pattern in the mathematical model, suggesting that LFPs have limited ability to precisely localize generators of transmembrane current flow. The PRAT-CSD profiles obtained by taking the second spatial derivative on the PRAT-LFPs are

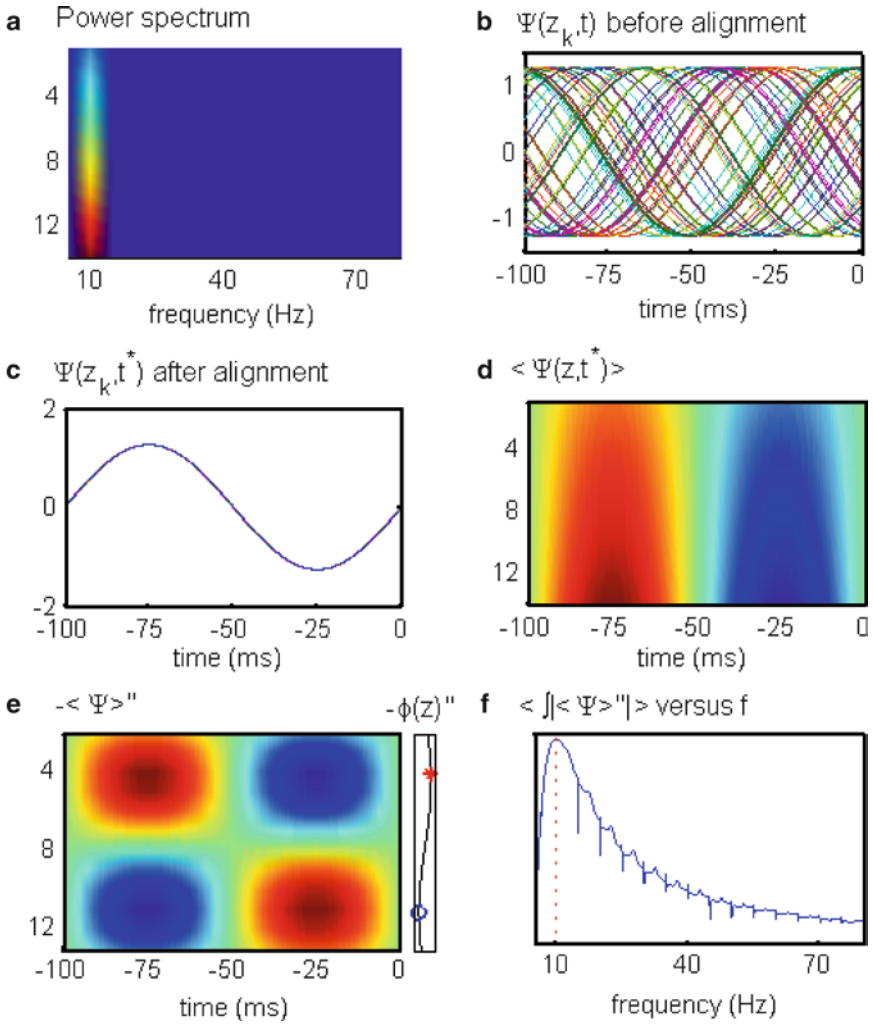

Fig. 1. Simulation example where the temporal dynamics is defined by a 10 Hz sinusoid. (**a**) Power spectra (5–80 Hz) as a function of electrode contact. (**b**) Trials from the reference contact before phase realignment. (**c**) The same trials after phase alignment. (**d**) The PRAT-LFP profile. (**e**) The PRAT-CSD profile. (**f**) The spectrum of the total transmembrane current flow. The horizontal axis is frequency (Hz) in (**a**) and (**f**). It is time otherwise in the unit of millisecond.

shown in Figs. 1e and 2e. The source and the sink pairs in the CSD profiles are clearly seen at around electrode contact 4 and 11. Temporally, the source-sink pair oscillates at a frequency of 10 Hz. Thus, the PRAT method recovers the dynamics built into the mathematical model. The above analysis can be carried out for each frequency from 5 to 80 Hz. Integrating the rectified PRAT-CSD profile over space and a given time interval yields the amount of transmembrane current at frequency *f*. The results are plotted in panel (f) and are called the CSD spectra. From the CSD spectrum, the greatest amount of transmembrane current is seen to occur at10 Hz. This again is in agreement with the conditions implemented in the mathematical model.

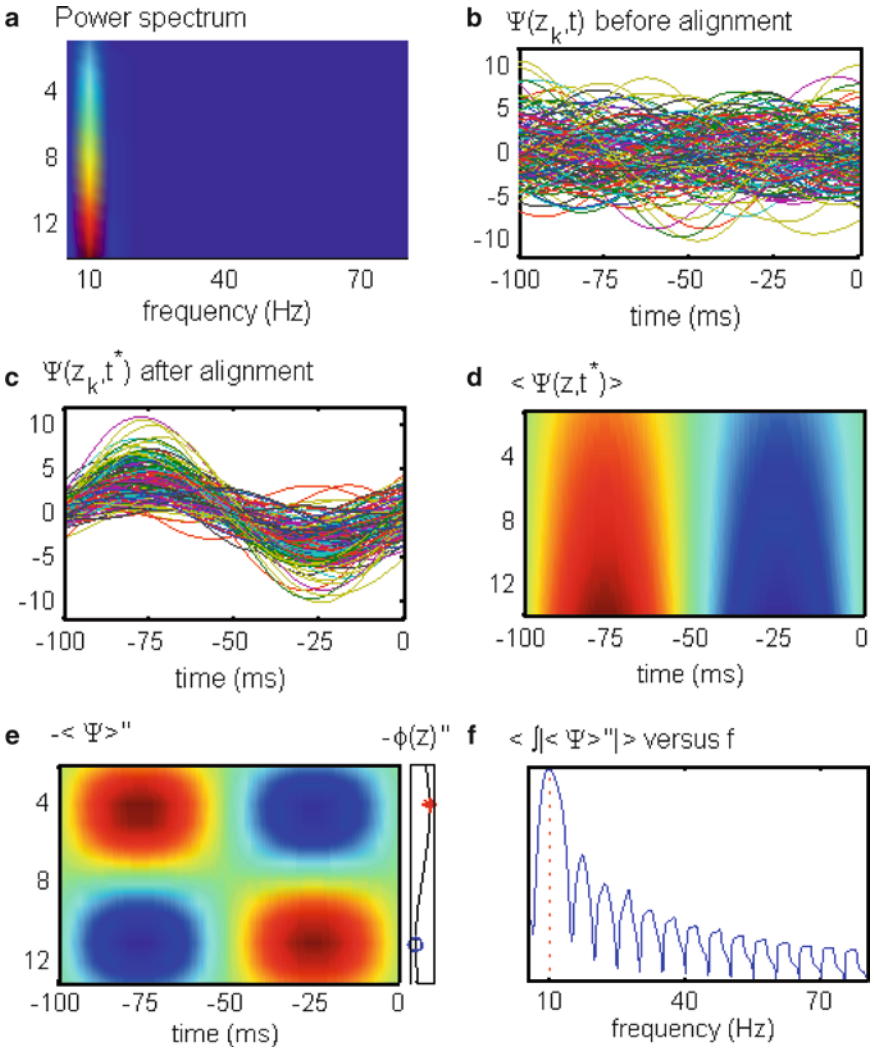

Fig. 2. Simulation example where the temporal dynamics is defined by an AR(2) process; the conventions are otherwise the same as in Fig. 1.

5. Application to Experimental Data

Field potential oscillations are ubiquitous in the nervous system. Depending on the signal rhythmicity, these oscillations are classified according to the following approximate nomenclature: delta (1–3 Hz), theta (4–7 Hz), alpha (8–12 Hz), beta (13–25 Hz), and gamma (25–90 Hz). The alpha rhythm is a prominent oscillatory activity in the 8–12 Hz band in EEG recordings over the occipital and parietal areas during wakefulness (16, 17). Nearly 80 years after its discovery (18), its genesis, cellular mechanisms, and functions remain unclear. Early work emphasized the pacemaking

role of the thalamus (19). More recent evidence suggests that it might be of a cortical origin (20). This problem is considered in this chapter by recording LFP and multiunit activity (MUA) from the inferotemporal cortex of a behaving macaque monkey. The PRAT method, in conjunction with other methods such as CSD-MUA coherence, is applied to address two problems: (1) laminar location of alpha current generators and (2) effect of prestimulus alpha oscillation on stimulus-evoked processing.

5.1. Experimental Paradigm

The data considered here is part of a previously published study (21, 22). A male macaque monkey was trained to discriminate stimuli in both visual and auditory domains. There are two conditions. In Condition 1, the monkey was presented with a mixed stream of auditory and visual stimuli. In each sensory modality, a standard stimulus occurred 86% of the time and an oddball stimulus 14% of the time. Selective attention was manipulated by instructing the monkey to respond to the oddball stimulus in the attended modality only. Task difficulty was balanced between the modalities. In Condition 2, the monkey performed the oddball detection task in the auditory domain in the absence of visual stimulation. The reason for analyzing activity in visual cortices during auditory discrimination was that the discrimination kept the monkey verifiably alert without using visual stimuli, so that we could study spontaneous ongoing neural activity.

5.2. Recordings

LFP and MUA were sampled with a linear array electrode with 14 contacts spanning all six cortical layers in the inferotemporal cortex. Data from one penetration, collected during periods of adequate task performance (i.e. >80% target detection), were analyzed to demonstrate the method presented above.

Problem 1: Laminar generators of ongoing alpha oscillation. Data from Condition 2 were analyzed. The length of a contiguous segment of spontaneous ongoing activity was on average 30 s long and there were five such segments for the penetration. After high-pass filtering (3 Hz, zero phase-shift) and down-sampling to 200 Hz, the LFP data were further divided into epochs of 200 ms in duration, which were considered trials or realizations of an underlying stochastic process. The power spectrum of each recording contact was estimated and the contact showing the highest power spectral density at 10 Hz was chosen as the reference channel. The PRAT method was used to obtain PRAT-LFP and PRAT-CSD. Figure 3a shows the results where the reference contact is channel 6. The PRAT-LFPs (solid lines) exhibit clear oscillation at 10 Hz. The PRAT-CSD (color coded) revealed an alpha current generator in the supra-granular layers (around contacts 5–7) with an underlying source/sink/source configuration. The alpha current generator in the infra-granular layers (around contact 10) was relatively weak. No alpha current generator was seen in the granular layer. The generator around contact three is believed to reflect

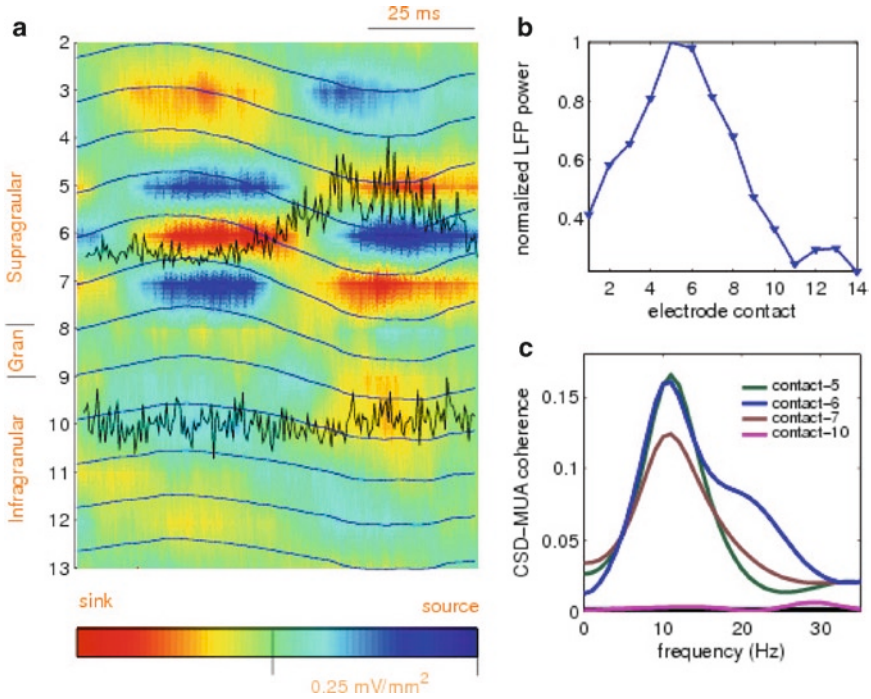

Fig. 3. Analysis of spontaneous alpha activity in inferotemporal cortex. (**a**) PRAT-CSD profile displayed as a color-coded plot, which is the second spatial derivative of the PRAT-LFPs (*solid traces*). A single epoch of MUA from two contacts is superimposed. (**b**) Laminar distribution of the peak (10 Hz) LFP power across recording contacts. (**c**) CSD-MUA coherence spectra at different contacts.

dendritic backpropagation. In Fig. 3b, the alpha band power is plotted as a function of the recording contact. The highest power occurs around channels 5 and 6, suggesting that the alpha current generator in the supra-granular layers may play an important role in the overall organization of alpha activity in the column.

The respective roles of the alpha current generators can be further delineated by examining the concomitant MUA data. In Fig. 3a, an epoch of MUAs at channels 6 and 10 are overlain on the CSD profile. The MUA near the supra-granular layer alpha generator varies rhythmically with the underlying current, while the MUA near the infra-granular alpha generator is not modulated by the current. This suggests that the alpha current generator in the supra-granular layers is possibly the pacemaker of the alpha rhythm in the column. We confirmed this impression by calculating the CSD-MUA coherence. The MUA data were epoched the same way as the LFP data and down-sampled from 2 kHz by taking a temporal average in nonoverlapping windows of 5 ms duration to achieve effectively the same sampling resolution of 200 Hz as the down-sampled LFPs. The coherence between single-trial CSDs around alpha current generators identified by the PRAT-CSD method and the corresponding mean-centered single-trial MUAs was calculated by the multivariate autoregressive

(MVAR) spectral analysis method (23). Figure 3c gives the CSD-MUA coherence at channels 5, 6, 7, and 10 where relatively high transmembrane current flows were found. In the supra-granular layers, the CSD-MUA coherence is relatively strong, reaching values close to 0.16, while in the infra-granular layers, the CSD-MUA coherence is close to zero. This supra-granular bias is consistent with the single epoch data in Fig. 3a.

The above results demonstrate that the inferotemporal cortex contains an alpha pacemaker in the supra-granular layers, in agreement with the suggestion that the alpha rhythm might be of a cortical origin. A more thorough analysis of this problem has been carried out by Bollimunta et al. (24). The alpha pacemaker in the supra-granular layers has a source/sink/source configuration. In light of the substantially enlarged basal dendritic arbor reaching the size of 400 μm in IT (25), this alpha generator most likely reflects the activity of superficial pyramidal neurons. The CSD-MUA coherence further suggests basal dendritic excitation. It is worth noting that Lukach et al. (26), in an in vitro slice study, have shown that the supra-granular layers contain the pacemaker of alpha range oscillations in the entorhinal cortex in rats.

Problem 2: Effect of prestimulus alpha oscillation on stimulus evoked response. The data recorded under Condition 1 were considered. The continuous LFP recordings were divided into 600 ms (–200, 400 ms) epochs based on the standard visual stimulus triggers. The prestimulus interval was defined to be from –200 to 0 ms, where 0 ms denotes stimulus onset. After data preprocessing, approximately 2,000 trials during which the monkey paid attention to the visual stimulus were made available for further analysis. The stimulus-evoked CSD from contact 5 in the supra-granular layers was computed using the conventional method and shown in Fig. 4. From this figure, an early stimulus processing

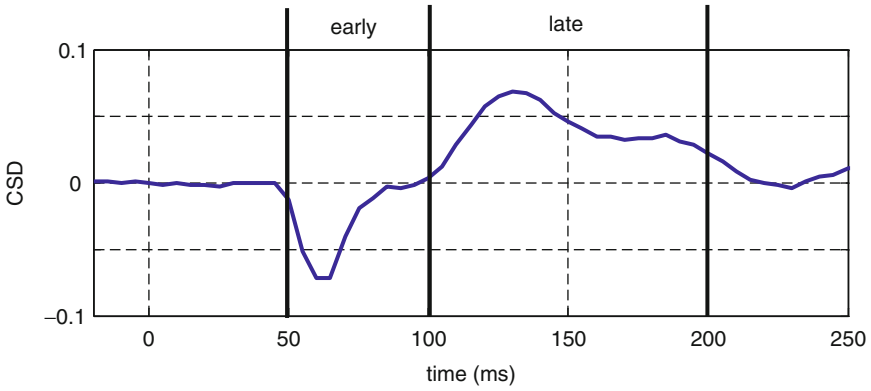

Fig. 4. Stimulus evoked current source density from a contact in the supra-granular layers. Early and late evoked responses are marked.

period (50–100 ms) and a late processing period (100–200 ms) were defined. Figure 5a shows the CSD profile of the ongoing prestimulus alpha oscillation determined by the PRAT method. Note the similarity between the CSD profile in Fig. 5a and that in Fig. 3a. Although obtained under different experimental conditions, these transmembrane current flow patterns are likely to reflect the same physiological generating mechanisms.

To examine the relation between prestimulus alpha oscillation and stimulus-evoked response, the magnitude of the prestimulus oscillation at 10 Hz was estimated on a trial-by-trial basis. A template matching method was used for this purpose. For single-trial LFP data, the second spatial derivative see (3) was calculated to yield single-trial CSD profiles. The PRAT-CSD in Fig. 5a was used as a template and moved along a given single-trial

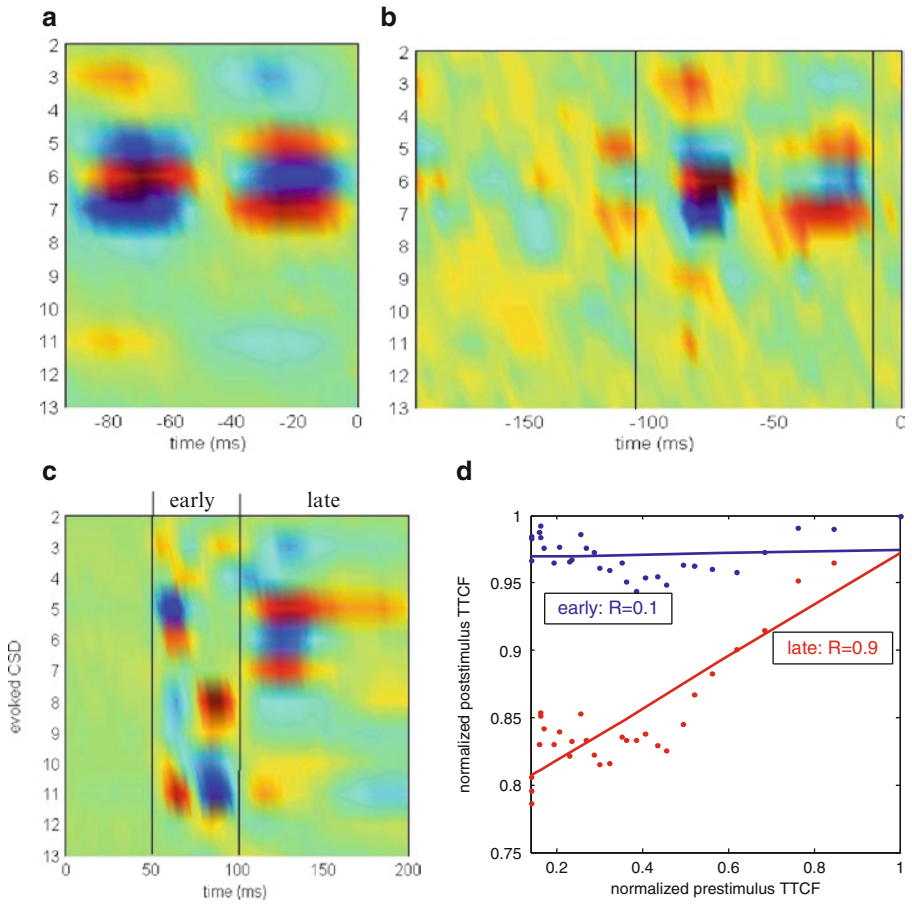

Fig. 5. Effect of prestimulus alpha oscillation on stimulus-evoked response. (**a**) PRAT-CSD profile at 10 Hz during the prestimulus time period, which is used as a template for measuring the strength of single-trial alpha activity. (**b**) A trial having a strong match index value with the template (note the CSD pattern between the two *solid lines*). (**c**) Stimulus evoked CSD profile. (**d**) Early (*blue*) and late (*red*) evoked responses plotted against the normalized magnitude of prestimulus alpha oscillation. Here TTCF stands for total transmembrane current flow.

CSD profile to find the best pattern match defined in terms of cross correlation. The correlation coefficient at the best match location was retained as an index of the magnitude of the prestimulus alpha activity in that trial. The procedure was repeated for all trials. Figure 5b shows a single-trial CSD profile with a high matching index value; the similarity between the transmembrane current flow pattern that is between the two vertical lines and the PRAT-CSD in Fig. 5a is noticeable. All the trials were sorted into groups of 500 trials, according to the values of the template matching index, each group having 90% of the trials overlapped with the previous one, starting from the lower matching index value to the highest. For the 500 trials in each group, a PRAT procedure was performed to yield a group PRAT-CSD profile. The total transmembrane current flow (TTCF) was computed by integrating the rectified ongoing laminar CSD over time (100 ms) and space (depth). For the same group of trials, the stimulus-evoked CSD profile, shown in Fig. 5c, was calculated in the conventional way. The TTCF during the early (50–100 ms) and the late (100–200 ms) poststimulus time period were obtained and plotted against the prestimulus alpha TTCF in Fig. 5(d) (blue for early and red for late). All quantities were normalized to a maximum value of 1. The solid straight lines represent least squares fits. The correlation coefficient between prestimulus alpha activity and the early evoked response is 0.1, while the correlation coefficient between prestimulus alpha activity and the late component is 0.9.

The above results demonstrate that the magnitude of the prestimulus alpha oscillation can affect stimulus processing. In particular, the prestimulus alpha oscillation is shown to be more strongly correlated with the late evoked component than the early evoked component. This observation appears to contradict intuitive expectations and thus calls for a possible explanation. In the cortex, excitatory neuronal information transmission is mediated by the release of the neurotransmitter glutamate. There are two major classes of glutamate receptors: AMPA and NMDA. On the one hand, experimental evidence suggests that the early evoked component reflects the fast response to stimulus input and is mainly mediated by AMPA receptors (27, 28). On the other hand, the late evoked component is apparently related to neuronal responses to feedback input from higher order areas and is thought to engage the NMDA receptors (28, 29). Spontaneous field potential oscillations in the theta and alpha range before the onset of stimulus reflect the cyclical variation in the excitability of neuronal ensembles (30–33). They involve the potentiation of NMDA receptors (34–36). The NMDA-mediated increase in excitability is an essential ingredient in recent theories of attention and memory (29, 37). This differential involvement of glutamate receptors with distinct stages of information processing

and prestimulus facilitation of NMDA receptors may underlie the correlation pattern observed between prestimulus ongoing alpha activity and stimulus evoked response.

Acknowledgment

This work was supported by NIH grants MH070948, MH079388, and MH060358.

References

1. Mitzdorf U (1985) Current source density method and application in cat cerebral cortex: investigation of evoked potentials and EEG phenomenon. Physiol Rev 65:37–100.
2. Nakagawa H, Matsumoto N (2000) Current source density analysis of ON/OFF channels in the frog optic tectum. Prog Neurobiol 61:1–44.
3. Nicholson C, Freeman JA (1975) Theory of current source-density analysis and determination of conductivity tensor for anuran cerebellum. J Neurophysiol 38:356–368.
4. Schroeder CE, Steinschneider M, Javitt DC, Tenke CE, Givre SJ, Mehta AD, Simpson GV, Arezzo JC, Vaughan HG (1995) Localization of ERP generators and identification of underlying neural processes. Electroencephalogr Clin Neurophysiol Suppl 44:55–75.
5. Liang H, Bressler SL, Ding M, Truccolo WA, Nakamura R (2002) Synchronized activity in prefrontal cortex during anticipation of visuomotor processing. Neuroreport 13:2011–2015.
6. Zhang Y, Wang X, Bressler SL, Chen Y, Ding M (2008) Prestimulus cortical activity is correlated with speed of visuomotor processing. J Cogn Neurosci 20(10):1915–1925.
7. Pitts W (1952) Investigations on synaptic transmission. In: Cybernetics: transactions of the ninth conference. von Foerster H (Ed), Josiah Macy Jr. Foundation, New York, pp 159–166.
8. Howland B, Lettvin JY, McCulloch WS, Pitts W, Wall PD (1955) Reflex inhibition by dorsal root interaction. J Neurophysiol 18:1–17.
9. Freeman JA, Nicholson C (1975) Experimental optimization of current source-density technique for anuran cerebellum. J Neurophysiol 38:369–382.
10. Hämälainen M, Hari R, Ilmoniemi RJ, Knuutila J, Lounasmaa OV (1993) Magnetoencephalography – theory, instrumentation, and applications to noninvasive studies of the working human brain. Rev Modern Phys 65:413–497.
11. Csicsvari J, Jamieson B, Wise K, Buzsaki G (2003) Mechanisms of gamma oscillations in the hippocampus of the behaving rat. Neuron 37:311–322.
12. Rangarajan G, Ding M (2000) Integrated approach to the assessment of long range correlation in time series data. Phys Rev E 61:4991–5001.
13. Buzsaki G, Draguhn A (2004) Neuronal oscillations in cortical networks. Science 304: 1926–1929.
14. Freeman WJ, Rogers LJ, Holmes MD, Silbergeld DL (2000) Spatial spectral analysis of human electrocorticograms including the alpha and gamma bands. J Neurosci Methods 95:111–121.
15. O'Connor SC, Robinson PA (2004) Unifying and interpreting the spectral wavenumber content of EEGs, ECoGs, and ERPs. J Theor Biol 231:397–412.
16. Shaw JC (2003) Brain's alpha rhythm and the mind. Elsevier, Amsterdam
17. Niedermeyer E (2005) The normal EEG of the waking adult. In: Electroencephalography: basic principles, clinical applications and related fields. Niedermeyer E (Ed), Williams and Wilkins, Baltimore, pp 149–173.
18. Berger H (1929) Über das elektroencephalogramm des menschen (On the electroencephalogram of man). Arch Psychiatr Nervenkr 87:527–570.
19. Andersen P, Andersson SA (1968) Physiological basis of the alpha rhythm. Appleton-Century-Crofts, New York
20. Lopes da Silva FH, Vos JE, Mooibroek J, Van Rotterdam A (1980) Relative contributions of intracortical and thalamo-cortical processes in the generation of alpha rhythms, revealed by

partial coherence analysis. Electroencephalogr Clin Neurophysiol 50:449–456.

21. Mehta AD, Ulbert I, Schroeder CE (2000a) Intermodal selective attention in monkeys. I. Distribution and timing of effects across visual areas. Cereb Cortex 10:343–358.
22. Mehta AD, Ulbert I, Schroeder CE (2000b) Intermodal selective attention in monkeys. II. Physiological mechanisms of modulation. Cereb Cortex 10:359–370.
23. Ding M, Bressler SL, Yang W, Liang H (2000). Short-window spectral analysis of cortical event-related potentials by adaptive multivariate autoregressive modeling: data preprocessing, model validation, and variability assessment. Biol Cybern 83:35–45.
24. Bollimunta A, Chen Y, Schroeder CE, Ding M (2008) Neuronal mechanisms of cortical alpha oscillations in awake-behaving macaques. J Neurosci 28(40):9976–9988.
25. Elston GN, Tweedale R, Rosa MGP (1999) Cortical integration in the visual system of the macaque monkey: large-scale morphological differences in the pyramidal neurons in the occipital, parietal and temporal lobes. Proc R Soc Lond 266:1367–1374.
26. Lukatch HS, MacIver MB (1997) Physiology, pharmacology, and topography of cholinergic neocortical oscillations in vitro. J Neurophysiol 77:2427–2445.
27. Hackley SA (1993) An evaluation of the automaticity of sensory processing using event-related potentials and brain-stem reflexes. Psychophysiology 30:415–428.
28. Roelfsema PR, Ooyen A (2005) Ation-gated reinforcement learning of internal representations for classification. Neural Comput 17: 2176–2214.
29. Schroeder CE, Mehta AD, Foxe JJ (2001) Determinants and mechanism of attention modulation of neural processing. Front Biosci 6:672–684.
30. Bishop G (1933) Cyclic changes in excitability of the optic pathway of the rabbit. Am J Physiol 103:213–224.
31. Steriade M, Nunez A, Amzica F (1993) A novel slow oscillation of neocortical neurons in vivo: depolarizing and hyperpolarizing components. J Neurosci 13:3252–3265.
32. Sanchez-Vives MV, McCormick DA (2000) Cellular and network mechanisms of rhythmic recurrent activity in neocortex. Nat Neurosci 3:1027–1034.
33. Lakatos P, Shah AS, Knuth KH, Ulbert I, Karmos G, Schroeder CE (2005) An oscillatory hierarchy controlling neuronal excitability and stimulus processing in the auditory cortex. J Neurophysiol 94:1904–1911.
34. Silva LR, Amitai Y, Connors BW (1991) Intrinsic oscillations of neocortex generated by layer 5 pyramidal neurons. Science 251:432–435.
35. Flint AC, Connors BW (1996) Two types of network oscillations in neocortex mediated by distinct glutamate receptor subtypes and neuronal populations. J Neurophysiol 75:951–956.
36. Placantonakis DG, Welsh JP (2001) Two distinct oscillatory states determined by the NMDA receptor in rat inferior olive. J Physiol 534:123–140.
37. Vertes RP (2005) Hippocampal theta rhythm: a tag for short term memory. Hippocampus 15:923–935.

http://www.springer.com/978-1-60327-201-8

Electrophysiological Recording Techniques
Vertes, R.P.; Stackman, Jr., R.W. (Eds.)
2011, XIV, 284 p., Hardcover
ISBN: 978-1-60327-201-8
A product of Humana Press